Japanese Journal of Applied Physics
Vol. 46, No. 7A, 2007, pp. 4276–4281

Initial Trial of Plasma Mass Separation by Crossed Electric and Magnetic Fields

Shunjiro SHINOHARA* and Seiichi HORII

Interdisciplinary Graduate School of Engineering Sciences, Kyushu University, Kasuga, Fukuoka 816-8580, Japan

(Received August 30, 2006; revised November 16, 2006; accepted March 19, 2007; published online July 4, 2007)

Using segmented concentric rings to produce a radial electric field, an initial trial experiment on ion mass separation in a magnetized plasma with low collisionality has been successfully carried out. With the increase in electric field or the decrease in magnetic field, the azimuthal flow velocity in the Xe plasma saturated and then it decayed due to the unconfined condition. On the other hand, the Ar plasma, whose mass is lighter than the Xe one, did not show this behavior in this operational region. These results are consistent with a particle orbit analysis and a simple calculation of the balances of forces.
[DOI: 10.1143/JJAP.46.4276]

KEYWORDS: plasma, rotation, mass separation, biasing, electric field, magnetic field

1. Introduction

Plasma flow with associated instabilities has been the subject of interest of many studies, and the structural formation of electric fields and a bifurcation have been major concerns in connection with this flow in, e.g., space plasma,[1)] nuclear fusion related to enhanced confinement with the shear of $\mathbf{E} \times \mathbf{B}$ rotation ($\mathbf{E}$: electric field, $\mathbf{B}$: magnetic field)[2,3)] and application fields.[4)] These plasmas often exhibit inherent, similar, and universal characteristics such as nonlinear self-organizing phenomena, under different parameter regimes. Concerning rotating plasmas in an axial magnetic field, historically, Q-machines[5,6)] showed instabilities brought about by changing the $\mathbf{E}$ profile leading to a velocity shear. Probe biasing (voltage) has been attempted to modify the potential profile, relating to velocity shear, in a tokamak[7)] in terms of enhanced confinement. In mirror devices, the stabilization of low-frequency instabilities and wave excitation with a strong shear has been realized along with bistable density transitions by voltage biasing.[8–16)] Recently, by this biasing scheme, toroidal rotation has also been studied with an internal ring trap device.[17)]

However, in contrast to this active research, there have been few experiments[14,18–21)] to show a large change of the density profile with high azimuthal rotation velocity in a controlled manner by biasing to multiple electrodes from a fundamental viewpoint. Controlling the radial electric field to change this velocity is a critical issue in the various fields mentioned above, and one of the most important subjects utilizing this method is isotope separation:[22)] Plasma isotope separation utilizes, e.g., calutron,[22)] atomic vapor laser isotope separation,[23)] ion cyclotron heating,[24)] rotation plasma (centrifuge),[25)] and gas discharges.[26)] Since the small annual productivity is a problem, finding an effective method of mass separation is still a scientific and technological task. In the rotation plasma, in spite of a model proposed on the basis of simple formulae, e.g., refs. 8, 27, and 28, this subject has been scarcely investigated experimentally,[29,30)] using our developed technique of biasing mentioned above, e.g., refs. 18 and 19, and this proof-of-principle experiment should be advanced in more detail. In this paper, we present the basic characteristics of plasma profiles influenced by an electric field, using two different gas species: the results lead to an initial demonstration of ion mass separation. Here, the control of the crossed magnetic and the electric fields, where the latter is generated by biasing ten concentric rings,[19)] was attempted, to change the ion orbit trajectories between two kinds of ions: Ar and Xe. A simple consideration of balances of forces and a particle orbit analysis also support the experimental results.

This paper is organized as follows. In §2, we describe our experimental setup to produce and rotate a plasma column briefly, as well as a simple ion orbit analysis. In §3, we present experimental results on different behaviors of Ar and Xe ions under the control of the electric field in the presence of the magnetic field. Finally, in §4, the results are summarized.

2. Experimental Setup and Ion Orbit Analysis

First, we briefly show the experimental setup in Fig. 1, since the details of our device are described in refs. 15 and 20. Ar and Xe plasmas with a pressure of ~0.16 mTorr (low collisionality condition: the electron mean free path is larger than the device length) were produced by a four-turn spiral antenna.[31,32)] The continuous output rf power and frequency of $P_{\mathrm{rf}} = 160\,\mathrm{W}$ and $f_{\mathrm{rf}} = 7\,\mathrm{MHz}$, respectively, were applied to a linear device, 44.5 cm in inner diameter and 170 cm in axial length. Here, (x, y, z) coordinates in the cylindrical system are shown in this figure. In order to control the radial potential profile, and thus the electric field profile, we used ten concentric, segmented rings, as biased electrodes. The inner and outer diameters of the n-th ring (in order from the center) were $4n - 4.6\,\mathrm{cm}$ ($2 \leq n \leq 10$) and $4n\,\mathrm{cm}$ ($1 \leq n \leq 10$), respectively. The spatial plasma parameters, such as the electron density n_{e}, electron temperature T_{e}, floating potential V_{f}, and azimuthal flow velocity v_θ, were measured by scanning the Langmuir probes including the Mach probe. In a typical target plasma, n_{e} was in the range of 2.5×10^9–$1.4 \times 10^{10}\,\mathrm{cm}^{-3}$ with $T_{\mathrm{e}} = 3$–$6\,\mathrm{eV}$ and estimated ion temperature $<1\,\mathrm{eV}$.

Next, ion orbit analysis was conducted in order to determine the experimental conditions after theoretical consideration of the escape of ions from the bulk plasma. In a cylindrical coordinate system (r, θ, z), from the radial force balance in the presence of both the radial electric field E_r and the axial magnetic field B_z, the azimuthal rotation velocity v_θ is written as follows.[8,27,28)]

*Corresponding author. E-mail address: sinohara@aees.kyushu-u.ac.jp

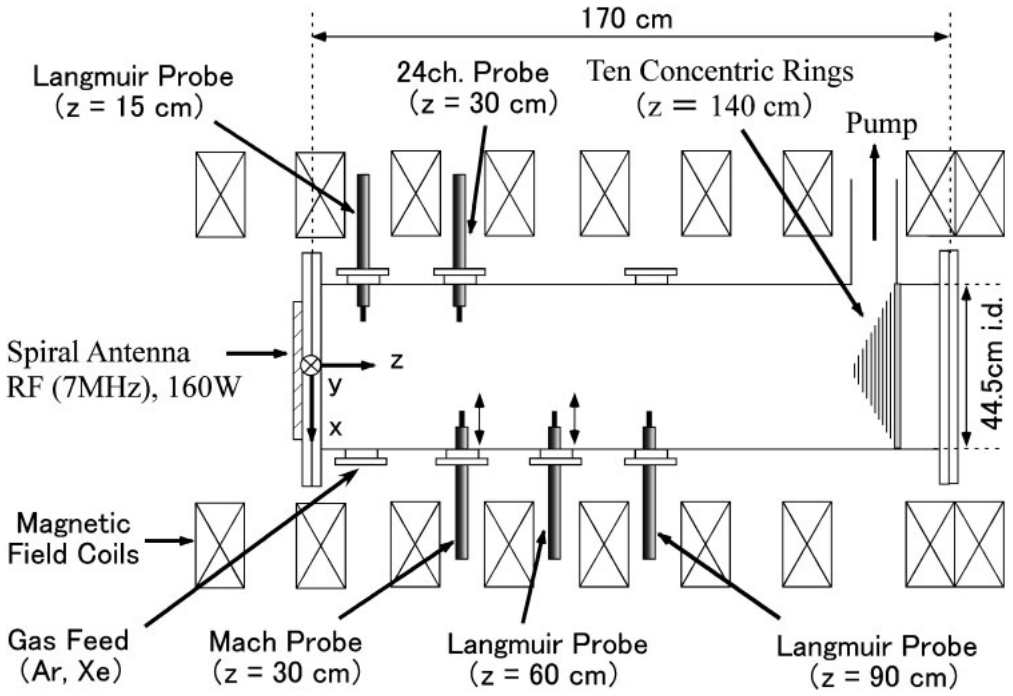

Fig. 1. Schematic view of experimental setup.

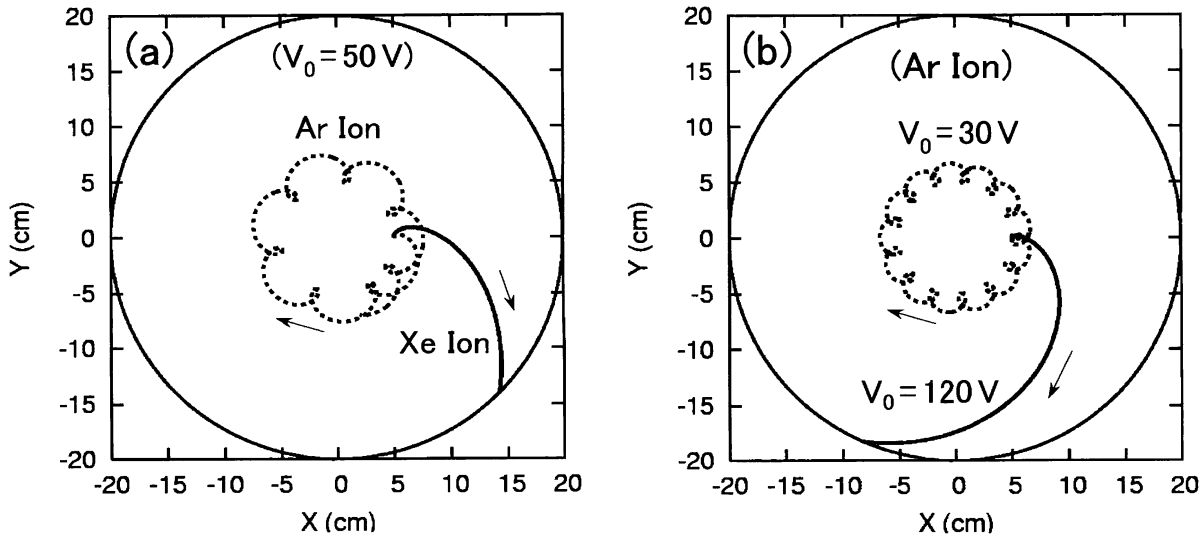

Fig. 2. Calculation of (a) Ar and Xe trajectories with $V_0 = 50\,\mathrm{V}$ and (b) Ar trajectories with $V_0 = 30$ and 120 V. Here, $B = 1{,}000\,\mathrm{G}$ and $a = 20\,\mathrm{cm}$, and $T_\mathrm{i} = 0.2\,\mathrm{eV}$ is assumed.

$$v_\theta = \frac{\omega_{\mathrm{ci}} r}{2}\left(-1 \pm \sqrt{1 - 4E_r/rB_z\omega_{\mathrm{ci}}}\right) \tag{1}$$

Here, ω_{ci} is the ion cyclotron angular frequency, and in deriving this equation, ion pressure gradient ∇p_i and ion–neutral collision frequency ν_{in} (see, e.g., ref. 33 for cross section data) terms are neglected because of the low ion temperature and low filling pressure: typical values of $(\nabla p_\mathrm{i}/n_\mathrm{i})/ev_\theta B_z$ and $(\nu_{\mathrm{in}}/\omega_{\mathrm{ci}})^2$ are estimated to be less than 0.01 and 0.001, respectively (n_i: ion density). When the component in the square root is negative, ions cannot be confined and a ballistic-like trajectory instead of the Larmor motion is expected (see Fig. 2). If the electric potential V has a parabolic profile, $V = V_0[1 - (r/a)^2]$ (V_0: central voltage, a: plasma radius), the critical atomic mass m_c, derived from the zero condition in the square-root part in eq. (1), is written as follows.[28)]

$$m_\mathrm{c} = ea^2B_z^2/8V_0 \tag{2}$$

Here, the ion with the atomic mass m being larger than m_c can escape from the plasma column (e: the electric charge). From this formula with the fixed plasma radius, m_c can be controlled by two parameters: B_z and V_0.

Figure 2(a) shows an example of the calculation of the Ar and Xe ion orbits with $V_0 = 50\,\mathrm{V}$, $B = 1{,}000\,\mathrm{G}$, $a = 20\,\mathrm{cm}$, and an assumed ion temperature of $T_\mathrm{i} = 0.2\,\mathrm{eV}$ in the Cartesian coordinate system. Here, the starting points of both ions were $(X, Y) = (5\,\mathrm{cm}, 0\,\mathrm{cm})$ and ion orbits were derived using the particle equation of motion. The leap-frog method, e.g., see ref. 34, was employed with the time step of

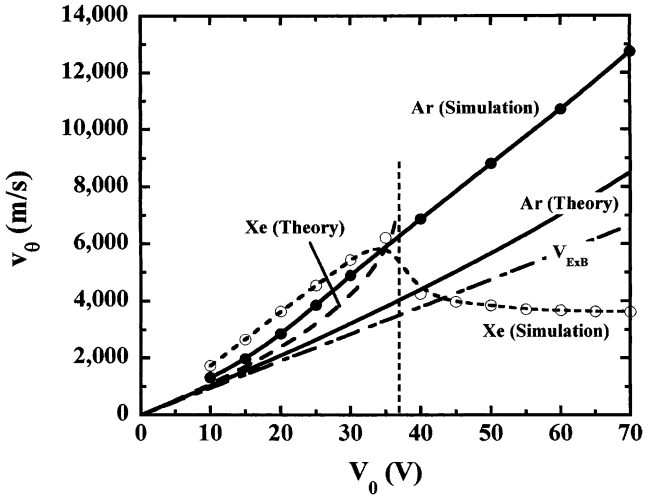

Fig. 3. Azimuthal Ar and Xe ion velocities at $r = 19\,\mathrm{cm}$ with $B = 1{,}000\,\mathrm{G}$, as a function of central bias voltage V_0. Here, a solid line with closed circles and a dotted line with open circles show cases of Ar and Xe ions, respectively, predicted by the particle orbit calculation (simulation). For comparison, $\mathbf{E} \times \mathbf{B}$ drift velocity (chain line) and the theoretical velocities obtained using the positive term in eq. (1) (solid and dashed lines show cases of Ar and Xe ions, respectively) are also shown. A vertical dotted line indicates a critical voltage $V_0 = 36.6\,\mathrm{V}$ of Xe ions.

$(2\pi/360)/\omega_{ci}$ to arrive at a stable solution. In Fig. 2(a), m_c from eq. (2) is $96m_p$ (m_p: proton mass), which lies between the Ar and Xe atomic masses of 40 and 131, respectively. In other words, the critical voltage of V_0 for Ar ions to escape from the plasma is 119 V with other parameters fixed. Whereas Ar ions are trapped, Xe ions are not confined. Figure 2(b) shows another example of controlling Ar ion orbits under confined and unconfined conditions, by changing V_0: $V_0 = 30$ and 120 V correspond to $m_c = 160m_p$ and $40m_p$ (almost equal to the mass of Ar), respectively. This ion orbit analysis is consistent with the ion confinement condition from eq. (2), which shows the controllability of ion mass separation.

Figure 3 shows the estimated v_θ of Ar and Xe ions, taken at $r = 19\,\mathrm{cm}$ with $B = 1{,}000\,\mathrm{G}$, as a function of V_0 as obtained by the particle orbit analysis along with theoretical values based on from eq. (1) (positive term) and $\mathbf{E} \times \mathbf{B}$ drift. Here, in the particle analysis, the starting points are in the inner region of the plasma column and the velocity is averaged over the particles with changing initial velocity angle: in steps of 10° with respect to the X-axis. Therefore, the result that the v_θ obtained by the simulation is higher than the theoretical one originates partly from the effect of the particles escaping from the inner plasma region: if the observation radius is fixed, e.g., $r = 19\,\mathrm{cm}$, v_θ coming from the inner region is higher, and this velocity does not change so much with increasing electric field if the initial starting radius is fixed.

In the small-applied-voltage area, i.e., $V_0 < 15\,\mathrm{V}$, $\mathbf{E} \times \mathbf{B}$ drift velocity is in good agreement with the theoretical v_θ obtained from eq. (1) for both ions. However, the discrepancy between two velocities is observed with the increase in V_0 for Xe ions, and v_θ obtained from eq. (1) goes to an infinite value at the critical voltage of $V_0 = 36.6\,\mathrm{V}$ (onset of the unconfined condition). From the simulation, v_θ goes up and saturates, then goes down near this critical voltage. On the other hand, Ar ions do not show any saturation of v_θ according to the particle analysis and also on the basis of eq. (1), but they are faster than the $\mathbf{E} \times \mathbf{B}$ drift velocity. These trends can be checked experimentally, which is described in the next section.

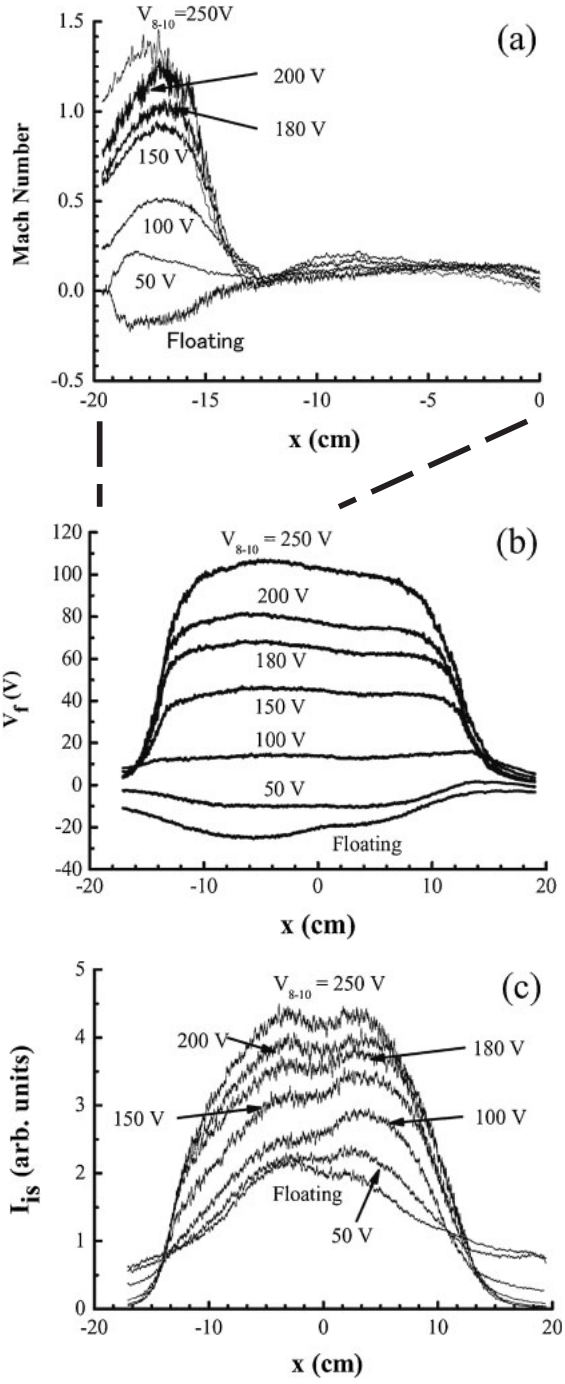

Fig. 4. Radial profiles of (a) Mach number, (b) floating potential V_f, and (c) ion saturation current I_{is} in the Ar plasma with $B = 1,200\,\mathrm{G}$, for various bias voltage V_{8-10}.

3. Results and Discussion

First, the different responses of Ar and Xe plasmas when changing the electric field are presented. Figures 4 and 5 show the radial profile of Mach number, floating potential V_f, and ion saturation current I_{is} when varying the bias voltage V_{8-10} in Ar and Xe discharges, respectively. Here,

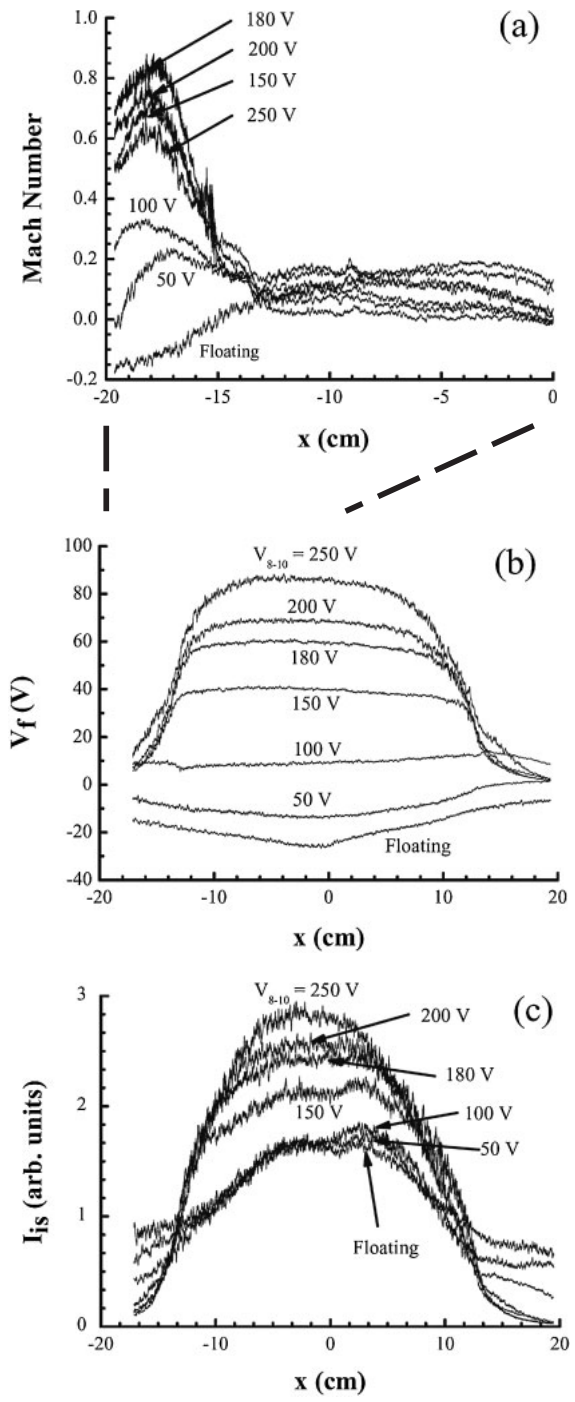

Fig. 5. Radial profiles of (a) Mach number, (b) floating potential V_f, and (c) ion saturation current I_{is} in the Xe plasma with $B = 1,200$ G, with changing bias voltage V_{8-10}.

V_{8-10} stands for the bias voltage applied to electrode nos. 8–10 (outer electrodes), with other electrodes being floated. Although the plasma potential was not measured, the electric field derived from V_f was not changed appreciably as long as T_e was nearly constant along the radius. In addition, since eV_f from Figs. 4 and 5 was much larger than kT_e (k: the Boltzmann constant), the experimental error due to the profile effect of T_e if any is considered to be small. The Mach number $M = 1$ and $I_{is} = 1$ correspond to a velocity of 3.5 (1.9) $\times 10^3$ m/s and an electron density of 2.9 (1.6) $\times 10^9$ cm^{-3} for Ar (Xe) ions, respectively, assuming $T_e = 5$ eV. In deriving the flow velocity by using the Mach probe, for convenience,[20,35] we used an unmagneitzed model[36] or a kinetic model[37] with zero viscosity, both of which have the same conversion coefficient. Even if the estimated velocity may be different from the real one, the parameter dependence on the bias voltage obtained can be compared qualitatively with results from the simulation/theory shown later. In the Ar plasma, with the increase in V_{8-10}, V_f in the central region increased with steepening slope near the edge region [Fig. 4(b)], leading to the higher plasma rotation ($M > 1$), as is shown in Fig. 4(a). The increase (decrease) in I_{is} in the central (edge) region with increasing V_{8-10}, and thus the density profile peaking, was observed in Fig. 4(c), which is consistent with the previous result.[14,19,20]

On the other hand, the Xe rotation velocity in Fig. 5(a) saturated at $V_{8-10} = 180$ V and then it decayed with the further increase in V_{8-10}, while V_f and I_{is} in Figs. 5(b) and 5(c), respectively, showed roughly the same behaviors as those of the Ar plasma: monotonic change of parameters with the bias voltage. Concerning the I_{is} profile, the following was expected: I_{is} decreases markedly in the region exceeding the critical electric field, and the decay of I_{is} further beyond this region becomes weaker as a result of the ballistic-like untrapped ion trajectory, mainly due to the localized potential profiles. Although this feature was not clearly observed, the experimental results indicated the above behavior: Ar plasma showed a monotonic decrease in I_{is} with increasing the bias voltage near the edge region. This is due to the direct ion loss having the enhanced ion orbit radius because of the relatively small ratio of the plasma radius to the effective ion Larmor one, which is pronounced near the edge region. On the other hand, Xe plasma showed the minimum ratio near the edge region at $V_{8-10} = 180$ V (near the critical field condition), and then increased a little with a weaker decay rate along the radial direction. Note that although the I_{is} profile indicated the expected behavior with increasing bias voltage, the saturation of the velocity in Xe discharges mentioned above clearly shows the threshold value for the ion confinement from the balance of forces and ion orbit analysis discussed above (its discussion using particle simulation is also presented later).

Next, in order to see this mass separation scheme more clearly, the magnetic field and the bias voltage were changed. Figure 6 shows the maximum flow velocity v_θ in the entire Ar or Xe plasma region as a function of ΔV_{max}. Here, ΔV_{max} denotes the maximum difference in floating potential V_f in the plasma. From this figure, the Ar plasma showed an increase in the velocity with ΔV_{max}, and ΔV_{max} values taking the maximum, saturated values of v_θ were ~40, ~60, and >100 V at $B = 800$, 1,000, and 1,200 G, respectively. On the other hand, the Xe plasma showed the saturation of v_θ at lower values of $\Delta V_{max} \sim 30$, ~ 33, and ~ 54 V at $B = 800$, 1,000, and 1,200 G, respectively, and the clear decay of the rotation velocity with the further increase in ΔV_{max} was observed. These behaviors are consistent with the above discussions.

Third, to explain the experimental results, we simulated the rotation velocity using the obtained potential profiles. Here, we approximated the plasma potential using a polygonal curve [three slopes: inflection points are $x = -8.2$, -12.5, and -17.5 (or -17) cm] under the assumption that the difference between the plasma and floating potentials

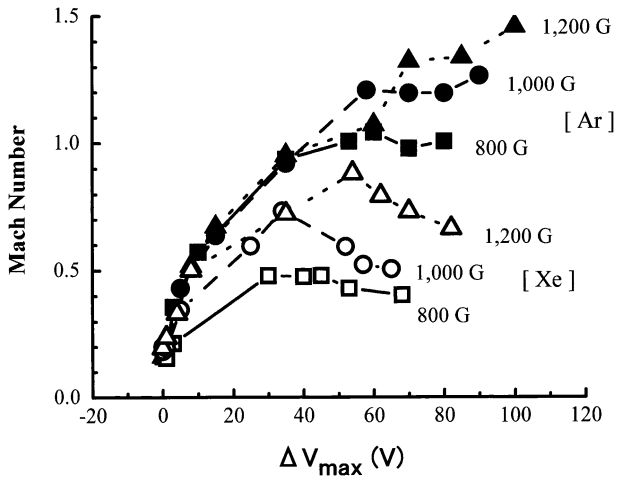

Fig. 6. Maximum Mach number as a function of ΔV_{max} in the Ar and Xe plasmas with $B = 800$, 1,000, and 1,200 G, with changing bias voltage as obtained from a particle simulation. Here, ΔV_{max} shows the voltage difference between the maximum and minimum floating potentials in the plasma.

is constant, i.e., a constant electron temperature along the radius. Basically, from this calculation, it was found that 1) the azimuthal rotation velocity profile was broad in the radial direction in the case of low bias voltages, 2) the maximum velocity was found near the edge of the strong electric field region ($x \sim -17$ cm) in the high-bias case, and 3) further away from this region, i.e., outside, this velocity decreased. Although the position of the maximum speed obtained was somewhat outside the strong-electric-field region [see 2)], 1) and 3) agree with the experimental results. Note that the peak position of v_θ can be determined from the following three factors: 1) v_θ coming from the inner region is faster, as was mentioned, 2) v_θ and v_r are dependent on the initial starting position and velocity, and 3) the electric field is weaker just near the edge. Therefore, near the outer edge region of the strong electric field, the maximum azimuthal velocity is expected.

In particular, in the Ar plasma, e.g., at $B = 1{,}200$ G, v_θ became 6,500 m/s at $x \sim -17$ cm with $\Delta V_{max} = 42$ V and the rate of increase of the velocity gradually decreased in the higher ΔV_{max} region. From the local satisfaction of zero value in the square root part of eq. (1), i.e., near the condition of velocity saturation, ΔV_{max} was estimated to be ~60, ~75, and ~100 V at $B = 800$, 1,000, and 1,200 G, respectively. In the Xe plasma, e.g., at $B = 1{,}200$ G, the rotation velocity reached a maximum value of 4,150 m/s with $\Delta V_{max} = 24$ V, and the further increase in ΔV_{max} led to a decrease in v_θ, e.g., 3,050 m/s with $\Delta V_{max} = 42$ V. From the local satisfaction of zero value in the square root part of eq. (1), ΔV_{max} was estimated to be ~17, ~20, and ~25 V at $B = 800$, 1,000, and 1,200 G, respectively. After exceeding the threshold electric field, where the maximum v_θ was observed, all ions are expelled out from the maximum-electric-field region in the simulation. These estimated values agreed with the experimental ones in Figs. 4–6 quantitatively within a factor of 2–3.

In our future study, in order to have more agreement, the rotation velocity should be measured accurately by a conventional spectroscopic method (determining a precise inversion profile is crucial since the emission light signal is the line-averaged value in this method) or by a sophisticated method of, e.g., the laser induced fluorescence (LIF) spectroscopy, and precise experimental determination of the plasma potential is necessary. Needless to say, control of the plasma potential profile by new methods, i.e., independent control of the plasma density and potential in the case of a small potential change, less than the threshold voltage (trapped conditions of particles), is also necessary. Then, discharges with a mixture of different gas species, when changing the electric field profile, should be attempted as the next step towards the fully realizing.

4. Conclusions

An initial trial experiment on ion mass separation by controlling an electric field has been successfully demonstrated in linear cylindrical magnetized plasma with low collisionality. With the increase (decrease) in electric (magnetic) field, the azimuthal flow velocity in the Xe plasma saturated and then it decayed due to the unconfined condition based on eq. (1), while the lighter Ar ions did not show this behavior in the operational region. These results are consistent with a particle orbit analysis using the particle equation of motion and a simple calculation of the balance of radial forces.

Acknowledgment

We would like to thank Professor Emeritus Y. Kawai for continuous encouragement.

1) D. N. Baker: Phys. Plasmas **6** (1999) 1700.
2) F. Wagner, G. Becker, K. Behringer, D. Campbell, A. Eberhagen, W. Engelhardt, G. Fussmann, O. Gehre, J. Gernhardt, G. v. Gierke, G. Haas, M. Huang, F. Karger, M. Keilhacker, O. Klüber, M. Kornherr, K. Lackner, G. Lisitano, G. G. Lister, H. M. Mayer, D. Meisel, E. R. Müller, H. Murmann, H. Niedermeyer, W. Poschenrieder, H. Rapp, H. Röhr, F. Schneider, G. Siller, E. Speth, A. Stäbler, K. H. Steuer, G. Venus, O. Vollmer, and Z. Yü: Phys. Rev. Lett. **49** (1982) 1408.
3) K. H. Burrell: Phys. Plasmas **4** (1997) 1499.
4) M. A. Lieberman and A. J. Lichtenberg: *Principles of Plasma Discharges and Materials Processing* (Wiley, New York, 1994).
5) G. I. Kent, N. C. Jen, and F. F. Chen: Phys. Fluids **12** (1969) 2140.
6) D. L. Jassby: Phys. Fluids **15** (1972) 1590.
7) R. J. Taylor, M. L. Brown, B. D. Frial, H. Grote, J. R. Liberati, G. J. Morales, P. Pribyl, D. Darrow, and M. Ono: Phys. Rev. Lett. **63** (1989) 2365.
8) A. Tsushima, T. Mieno, M. Oertl, R. Hatakeyama, and N. Sato: Phys. Rev. Lett. **56** (1986) 1815.
9) G. D. Severn, N. Hershkowitz, R. A. Breun, and J. R. Ferron: Phys. Fluids B **3** (1991) 114.
10) A. Mase, A. Itakura, M. Inutake, K. Ishii, J. H. Jeong, K. Hattori, and S. Miyoshi: Nucl. Fusion **31** (1991) 1725.
11) O. Sakai, Y. Yasaka, and R. Itatani: Phys. Rev. Lett. **70** (1993) 4071.
12) W. E. Amatucci, D. N. Walker, G. Ganguli, J. A. Antoniades, D. Duncan, J. H. Bowles, V. Gavrishchaka, and M. E. Koepke: Phys. Rev. Lett. **77** (1996) 1978.
13) M. Yoshinuma, M. Inutake, R. Hatakeyama, T. Kaneko, K. Hattori, A. Ando, and N. Sato: Fusion Technol. **35** (1999) 278.
14) S. Masuyama and S. Shinohara: J. Plasma Fusion Res. Ser. **4** (2001) 528.
15) S. Shinohara and S. Matsuyama: Phys. Plasmas **9** (2002) 4540.
16) S. Shinohara, Y. Nakamura, and S. Horii: Thin Solid Films **506–507** (2006) 564.
17) H. Saito, Z. Yoshida, H. Himura, J. Morikawa, and M. Fukao: Phys. Plasmas **11** (2004) 3331.
18) S. Shinohara, H. Tsuji, T. Yoshinaka, and Y. Kawai: Surf. Coat.

Technol. **112** (1999) 20.
19) S. Shinohara, N. Matsuoka, and Y. Yoshinaka: Jpn. J. Appl. Phys. **38** (1999) 4321.
20) S. Shinohara, N. Matsuoka, and S. Matsuyama: Phys. Plasmas **8** (2001) 1154.
21) S. Shinohara, N. Matsuoka, and S. Matsuyama: Trans. Fusion Technol. **39** (2001) 358.
22) M. W. Grossman and T. A. Shepp: IEEE Trans. Plasma Sci. **19** (1991) 1114.
23) T. Arisawa, Y. Suzuki, Y. Maruyama, and K. Shiba: J. Phys. D **15** (1982) 1955.
24) J. M. Dawson, H. C. Kim, D. Arnush, B. D. Fried, R. W. Gould, L. O. Heflinger, C. F. Kennel, T. E. Romesser, R. L. Stenzel, A. Y. Wong, and R. F. Wuerker: Phys. Rev. Lett. **37** (1976) 1547.
25) M. Krishnan, M. Geva, and J. L. Hirshfield: Phys. Rev. Lett. **46** (1981) 36.
26) E. F. Gorbunova, A. I. Karchevskii, and Yu. A. Muromkin: Sov. J. Plasma Phys. **12** (1986) 625.
27) A. Tsushima and N. Sato: J. Phys. Soc. Jpn. **60** (1991) 2665.
28) T. Ohkawa and R. L. Miller: Phys. Plasmas **9** (2002) 5116.
29) R. L. Miller, T. Ohkawa, S. F. Agnew, B. P. Cluggish, R. L. Freeman, J. Gilleland, S. Putvinski, L. Sevier, and K. R. Umstadter: Bull. Am. Phys. Soc. **46** (2001) 192.
30) B. P. Cluggish, F. Anderegg, R. L. Freeman, J. Gilleland, T. J. Hilsabech, R. C. Isler, W. D. Lee, A. Litvak, R. L. Miller, T. Ohkawa, S. Putvinski, K. R. Umstadter, and D. L. Winslow: Bull. Am. Phys. Soc. **48** (2003) 232.
31) S. Shinohara, S. Takechi, and Y. Kawai: Jpn. J. Appl. Phys. **35** (1996) 4503.
32) S. Shinohara, S. Takechi, N. Kaneda, and Y. Kawai: Plasma Phys. Control. Fusion **39** (1997) 1479.
33) A. V. Phelps: J. Phys. Chem. Ref. Data **20** (1991) 557.
34) E. J. Horowitz, D. E. Schumaker, and D. V. Anderson: J. Comput. Phys. **84** (1989) 279.
35) S. Shinohara: Phys. Plasmas **9** (2002) 1834.
36) M. Hudis and L. M. Lidsky: J. Appl. Phys. **41** (1970) 5011.
37) K.-S. Chung, I. H. Hutchinson, B. LaBombard, and R. W. Conn: Phys. Fluids B **1** (1989) 2229.